

Image Registration Using Implicit Similarity and Pixel Migration

A. Averbuch¹, Y. Keller^{1,2}

¹School of Computer Science, Tel Aviv University, Tel Aviv 69978
Israel

²Dept. of Electrical Engineering Systems
Tel-Aviv University
Tel-Aviv 69978, Israel

Abstract

This paper presents an energy minimization approach to the registration of significantly dissimilar images, acquired by sensors of different modalities. The proposed algorithm introduces a robust matching criterion by aligning the locations of gradient maxima. The alignment is formulated as a parametric variational optimization problem which is solved iteratively by considering the intensities of a single image. The locations of the maxima of the second image's gradient are used as initialization. Thus, an implicit matching criterion is achieved while utilizing the full spatial information, without resorting to invariant image representations. We are able to robustly estimate affine and projective global motions using 'coarse to fine' processing, even when the images are characterized by complex space varying intensity transformations. These cause current state-of-the-art algorithms to fail. Finally, we present results of registering real images, which were taken by multi-sensor and multi-modality using affine and projective motion models.

Keywords: Global motion estimation, multimodal images, multisensor images, gradient methods, image alignment

EDICS Category={2-ANAL, 2-MOTD}

1 Introduction

The registration of images acquired by sensors of different modalities is of special interest to remote sensing and medical imaging applications, as the information gained from such set of images is of a complementary nature. Proper fusion of the data obtained from the separate images requires accurate spatial alignment. This issue was extensively studied in the context of remote-sensing

(Sar, Flir, IR and optical sensors) [3, 4] and medical image registration (CT, MRI, UltraSound, MRA, DSA, CTA, SPECT, PET, fMRI, EEG, MEG, pMRI, fCT, EIT, MRE) [1, 2, 5]. Due to the different physical characteristics of the various sensors, the relationship between the intensities of matching pixels is often complex and unknown a-priori. Features present in one image might appear only partially in the other image or not appear at all, contrast reversal may occur in some image regions while not in others, multiple intensity values in one image may map to a single intensity value in the other image and vice versa. Furthermore, imaging sensors such as MRI, CT, SAR may produce significantly dissimilar images of the same scene when configured with different image processing parameters. Thus, the relationship between the input images can be modelled as

$$I_1(x, y) = T(I_2(\tilde{x}(x, y, \underline{P}), \tilde{y}(x, y, \underline{P})), x, y) \quad (1.1)$$

where $I_1(x, y)$ and $I_2(x, y)$ are images having some common overlap, \underline{P} is the global motion parameters vector and $T(\cdot)$ is the intensity mapping. Ordinary registration algorithms [6] assume $T \equiv 1$ and solve the registration problem by minimizing the L_2 norm:

$$\underline{P}^* = \arg \min_{\underline{P}} \left\{ \sum_{(x_1, y_1) \in S} \left(I_1(x_i^{(1)}, y_i^{(1)}) - I_2(\tilde{x}(x_i^{(1)}, y_i^{(1)}), \tilde{y}(x_i^{(1)}, y_i^{(1)}), \underline{P}) \right)^2 \right\} \quad (1.2)$$

For significantly dissimilar (multi-sensor) images, solving Eq. 1.2 does not result in image registration. A possible solution, used in prior works is to use representations of I_1 and I_2 (\hat{I}_1 and \hat{I}_2 respectively) which are invariant to brightness changes induced by the operator $T(\cdot)$ in Eq. 1.1. These representation include feature points [7], edge maps [8], oriented edge maps [3] and edge contours [4]. Matching is achieved using \hat{I}_1, \hat{I}_2 and either gradient methods [8], robust gradient methods [3], chain-code correlation [4] or geometrical hashing [9]. Gradient methods minimize the intensity discrepancies of \hat{I}_1 and \hat{I}_2 using an explicit similarity measure (usually the L_2 norm) and direct global optimization. This requires the discrepancies between \hat{I}_1 and \hat{I}_2 to be a smooth function of the motion parameters \underline{P} suitable for numerical differentiation. Since the process of creating invariant representations may result in important image information being lost, the optimization process may fail to converge. Geometrical matching techniques [4, 8, 9] align geometrical primitives such as feature points, contours and corners using vectorial geometric representations such as chain-codes and directional gradient maps [3]. Hence, these matchings are invariant to intensity changes once the geometrical primitives are detected. However, these algorithms can not be extended to global matching. Each geometrical primitive is matched on a single basis, resulting in poor global alignment and sensitively to outliers. The Mutual information registration algorithm [1, 2] estimates the global parametric transformation by maximizing a robust statistical similarity measure which is applied directly to the original image intensities I_1 and I_2 .

This paper offers an implicit similarity measure to address the limitations of the algorithms mentioned above, where the registration is achieved without defining a similarity measure and achieving its optimum. This measure achieves intensity invariant geometrical alignment while using robust global optimization. The algorithm aligns the set of pixels having large gradient magnitudes in both images. This set is invariant under most intensity changes and geometrical transformations. The alignment is achieved using a parametric minimization conducted using a **single** image where the second image’s pixel set is used as initiation. Hence, the convergence properties of the proposed algorithm depend on a single image which can be chosen to be the less noisy input image. This property makes the proposed algorithm especially suitable for multi sensor and multi modality registration where conventional image registration techniques may fail [3]. The method was successfully tested using image sets from remote sensing and medical multi sensor applications.

The paper is organized as follows: section 2 presents the pixel migration based image registration algorithm and its convergence is analyzed in Section 3. Experimental results are discussed in 4.

2 The image registration algorithm

State-of-the-art image registration techniques use explicit intensity similarity measures such as the L_1 and L_2 norms, whose optimization results in image alignment. In this section we formulate an implicit geometrical similarity measure suitable for robust multi sensor registration. Let $I_1(x, y)$ and $I_2(x, y)$ be the images which have some common overlap, then:

$$F(S(\underline{P})) \triangleq \sum_{(x_i, y_i) \in S_1(\underline{P})} |\nabla I_1(x_i, y_i)|^2 \quad (2.1)$$

where S_1 is a set of pixels in I_1 and maximizing $F(\underline{P})$ implies that the set S_1 consists mostly of image edges. Pixels having high gradient magnitudes correspond to primary structures within the image and their detection is robust. Contrary to high level geometric primitives such as contours and corners, no preset thresholds are needed.

2.1 Initial set detection

The set of pixels S_2 is detected in the first image by choosing the m pixels having the largest gradient magnitude. Usually we use 20% of the total image pixels.

2.2 Global alignment

Global alignment is achieved by minimizing the functional $F(\underline{P})$ defined in Eq. 2.1. Thus the problem is defined as:

$$\underline{P}^* = \arg \max_{\underline{P}} \{F(S(\underline{P}))\} \quad (2.2)$$

while the initial set $S_1(0)$ is given by:

$$S_1(0) = S_2(\underline{P}_0) \quad (2.3)$$

where:

- S_2 The set of coordinates of high gradient edge pixels detected in I_2
- $S_2(\underline{P})$ The set of S_2 coordinates projected according to the motion parameters vector \underline{P} : $S_2 = S_2(\underline{Q})$
- \underline{P}_0 An initial estimate of the motion parameters.

Hence, \underline{P}^* , the solution to Eq. 2.2, maps the set $S_1(\underline{P}^*)$ to the initial set S_2 and since the motion is assumed to be global, \underline{P}^* is an *implicit solution* to the image registration problem as no explicit similarity measure is used. Eq. 2.2 is solved using the intensity values of a **single** image, making the alignment process invariant to intensity changes. This process is presented in Figure 1.

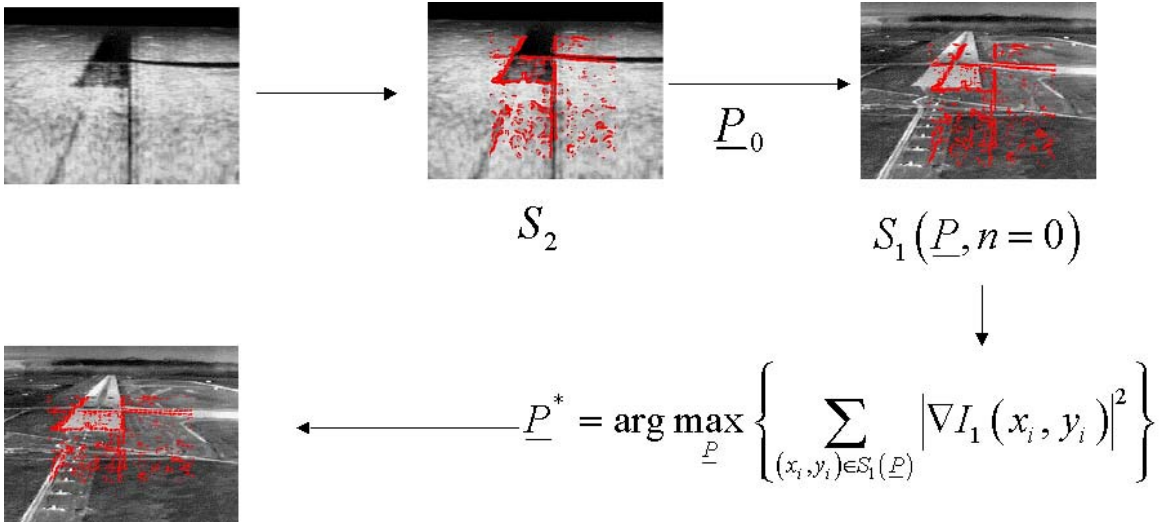


Figure 1: The multi-sensor registration algorithm flow. Clockwise starting at the upper-left corner: the second image. The high-gradient pixel set S_2 detected in the second image and overlaid on it. The set S_2 is projected onto the other image using the initial estimate \underline{P}_0 and named S_1 . The global optimization process leads to the alignment of S_1 .

2.3 Iterative optimization

Since $F(S_1(\underline{P}))$ is a non-linear function of \underline{P} , the motion parameters are computed by solving Eq. 2.2 using Newton's iterative optimization method [10].

The iterative refinement equation is given by:

$$\underline{P}_{n+1} = \underline{P}_n + \underline{\underline{H}}_{\underline{P}}^{-1} \nabla_{\underline{P}} F_n. \quad (2.4)$$

where $\nabla_{\underline{P}} F_n$ is the gradient vector of F in respect to \underline{P} at iteration n

$$\nabla F_i = \left[\frac{\partial F(x_i, y_i)}{\partial P_1} \quad \frac{\partial F(x_i, y_i)}{\partial P_2} \quad \cdots \quad \frac{\partial F(x_i, y_i)}{\partial P_m} \right]^T \quad (2.5)$$

and $\underline{\underline{H}}_{\underline{P}}^n$ is the Hessian matrix of F in respect to \underline{P} at iteration n

$$\underline{\underline{H}}_{\underline{P}}^n = \begin{bmatrix} \frac{\partial^2 F}{\partial P_1^2} & \frac{\partial^2 F}{\partial P_1 \partial P_2} & \cdots & \frac{\partial^2 F}{\partial P_1 \partial P_m} \\ \frac{\partial^2 F}{\partial P_2 \partial P_1} & \frac{\partial^2 F}{\partial P_2^2} & \cdots & \frac{\partial^2 F}{\partial P_2 \partial P_m} \\ & \vdots & \ddots & \\ \frac{\partial^2 F}{\partial P_m \partial P_1} & \frac{\partial^2 F}{\partial P_m \partial P_2} & \cdots & \frac{\partial^2 F}{\partial P_m^2} \end{bmatrix}. \quad (2.6)$$

In order to calculate $\nabla_{\underline{P}} F_n$ and $\underline{\underline{H}}_{\underline{P}}^n$ the derivative chain rule is used:

$$\begin{aligned} \nabla_{\underline{P}} f(x_i, y_i) &= \frac{\partial F(x_i, y_i)}{\partial P_j} \\ &= \frac{\partial F(x_i, y_i)}{\partial x} \frac{\partial x_i(x_i, y_i, \underline{P}_n)}{\partial P_j} + \frac{\partial F(x_i, y_i)}{\partial y} \frac{\partial y_i(x_i, y_i, \underline{P}_n)}{\partial P_j} \end{aligned} \quad (2.7)$$

$$\begin{aligned} \underline{\underline{H}}_{\underline{P}}(x_i, y_i) &= \frac{\partial \nabla_{\underline{P}} F(x_i, y_i)}{\partial P_j} \\ &= \frac{\partial \nabla_{\underline{P}} F(x_i, y_i)}{\partial x} \frac{\partial x_i(x_i, y_i, \underline{P}_n)}{\partial P_j} + \frac{\partial \nabla_{\underline{P}} F(x_i, y_i)}{\partial y} \frac{\partial y_i(x_i, y_i, \underline{P}_n)}{\partial P_j}. \end{aligned} \quad (2.8)$$

where $\nabla F(x_i, y_i)$ and $\underline{\underline{H}}_{\underline{P}}(x_i, y_i)$ are the gradient and Hessian in respect to P_j approximated at the i th pixel. \underline{P}_n is the parameters estimate after the n th iteration.

Thus, $\nabla_{\underline{P}} F_n$ and $\underline{\underline{H}}_{\underline{P}}$ are accumulated over the complete pixel set $S_1(\underline{P})$:

$$\nabla_{\underline{P}} F_n = \sum_{(x_i, y_i) \in S_1(\underline{P})} \nabla_{\underline{P}} F_n(x_i, y_i) \quad (2.9)$$

and

$$\underline{\underline{H}}_{\underline{P}} = \sum_{(x_i, y_i) \in S_1(\underline{P})} \underline{\underline{H}}_{\underline{P}}(x_i, y_i). \quad (2.10)$$

For motion models which are linear in respect to \underline{P}_n , such as the affine and projective models we have:

$$X_{Affine} = \begin{bmatrix} x & y & 1 & 0 & 0 & 0 \\ 0 & 0 & 0 & x & y & 1 \end{bmatrix} \quad (2.11)$$

and

$$X_{Projective} = \begin{bmatrix} x & y & 1 & 0 & 0 & 0 & \tilde{x}x & \tilde{x}y \\ 0 & 0 & 0 & x & y & 1 & \tilde{x}y & \tilde{y}y \end{bmatrix}. \quad (2.12)$$

The gradient vector and Hessian matrix can be expressed as:

$$\nabla_{\underline{P}} F_n = \sum_{(x_i, y_i) \in S_1(\underline{P})} X_i \nabla_{(x, y)} F_n(x_i, y_i) \quad (2.13)$$

$$\underline{\underline{H}}_{\underline{P}} = \sum_{(x_i, y_i) \in S_1(\underline{P})} X_i \underline{\underline{H}}_{(x, y)} X_i^T \quad (2.14)$$

where ∇F_n and $\underline{\underline{H}}$ are the gradient and Hessian in respect to the cartesian coordinate system:

$$\nabla F_n = \left[\begin{array}{cc} \frac{\partial F(x_i, y_i)}{\partial x} & \frac{\partial F(x_i, y_i)}{\partial y} \end{array} \right] \quad (2.15)$$

$$\underline{\underline{H}} = \left[\begin{array}{cc} \frac{\partial^2 F}{\partial x^2} & \frac{\partial^2 F}{\partial x \partial y} \\ \frac{\partial^2 F}{\partial y \partial x} & \frac{\partial^2 F}{\partial y^2} \end{array} \right] \quad (2.16)$$

Eq. 2.4 is iterated until either of the following convergence criteria is met:

1. A maximal (predefined) number of iteration is reached.
2. The update of the parameters becomes smaller than a predefined size.

2.4 Multiscale extension

In order to improve the convergence properties of the iterative algorithm in section 2.3, a resolution pyramid is constructed. The alignment algorithm starts at the coarsest resolution scale of the pyramid, then follows the subsequent levels in a coarse-to-fine approach. At each resolution scale, the calculation described in Section 2 is conducted where the results of the calculation at each scale serves as an initial guess for the finer iteration scale. Finally, when the procedure stops at the finest resolution scale, the final motion parameters are obtained.

The coarse-to-fine refinement process allows the alignment process to lock on a single dominant motion even when multiple motions are present. This motion, which is named *dominant motion*, is essential due to the presence of outlier feature points.

3 Convergence properties

The convergence properties of the proposed algorithm resemble those of regular gradient methods [11]. Hence, a sufficient convergence condition can be derived by analyzing the properties of the iterative refinement term in Eq. 2.4:

$$\underline{\Delta P}_n = \underline{H}_P^{-1} \nabla_P F_n \quad (3.1)$$

where $\underline{\Delta P}_n$ is the iterative refinement at iteration n .

The convergence does not depend on \underline{H}_P^{-1} which can be any positive-definite matrix, whose choice determines the convergence rate rather than the final values of the parameters.

3.1 Notation

Denote

S The set of pixels in I_1 .

$E\{S\}$ The expectancy of pixels within S .

S_1^n A subset of S - the set of pixels used at iteration n in I_1 to evaluate Eq. 2.1.

S_{Dom}^n A subset of S_1^n , the set of pixels in S_1^n having large gradient values corresponding to true alignment.

$E\{S_{Dom}^n\}$ The expectancy of pixels within S_{Dom}^n .

$\overline{S_{Dom}^n}$ A subset of S_1^n , the set of pixels in S_1^n having small gradient values corresponding to false alignment.

$E\{\overline{S_{Dom}^n}\}$ The expectancy of pixels within $\overline{S_{Dom}^n}$.

then

$$P(S_{Dom}^n) \triangleq P((x, y) \in S_{Dom}^n) = \frac{|S_{Dom}^n|}{|S|}, \quad (3.2)$$

$$P(\overline{S_{Dom}^n}) \triangleq P((x, y) \in \overline{S_{Dom}^n}) = \frac{|\overline{S_{Dom}^n}|}{|S|}, \quad (3.3)$$

and

$$P(S_1^n) \triangleq P((x, y) \in S_1^n) = \frac{|S_1^n|}{|S|}. \quad (3.4)$$

where $|S|$, $|S_{Dom}^n|$ and $|\overline{S_{Dom}^n}|$ are the sizes of S , S_{Dom}^n and $\overline{S_{Dom}^n}$ respectively.

3.2 Estimation of the pixels sets expectancies

The expectancies of the sets can be estimated by

$$\begin{aligned} E\{S\} &= E\{S_{Dom}^n\} P(S_{Dom}^n) + E\{\overline{S_{Dom}^n}\} (1 - P(S_{Dom}^n)) \\ &= E\{S_{Dom}\} \frac{|S_{Dom}|}{|S|} + E\{\overline{S_{Dom}^n}\} \frac{|S| - |S_{Dom}^n|}{|S|} \end{aligned} \quad (3.5)$$

assuming

$$|S| \gg |S_{Dom}| \quad (3.6)$$

we get

$$E\{S\} \approx E\{\overline{S_{Dom}^n}\} \quad (3.7)$$

and

$$E\{S_{Dom}\} \gg E\{S\}. \quad (3.8)$$

3.3 Spatial gradient expectancies estimation

The ratio of $E_{S_{Dom}^n}\{\nabla F_n\}$ and $E_{\overline{S_{Dom}^n}}\{\nabla F_n\}$ can be estimated by approximating the derivative ∇F is using finite differences

$$E\{\nabla F(x, y)\} = E\left\{\frac{\partial F}{\partial x}, \frac{\partial F}{\partial y}\right\} \quad (3.9)$$

where

$$\begin{aligned} E\left\{\frac{\partial F}{\partial x}\right\} &\simeq E\{F(x, y)\} - E\{F(x-1, y)\} \\ E\left\{\frac{\partial F}{\partial y}\right\} &\simeq E\{F(x, y)\} - E\{F(x, y-1)\} \end{aligned} \quad (3.10)$$

In particular, the expectancies $E_{S_{Dom}^n}\{\nabla F_n\}$ and $E_{\overline{S_{Dom}^n}}\{F_n\}$ can be estimated using Eqs. 3.7, 3.8 and 3.10

$$\begin{aligned} E\left\{\frac{\partial F}{\partial x} \mid (x, y) \in S_{Dom}\right\} &\simeq E\{S_{Dom}\} - E\{S\} \gg 0 \\ E\left\{\frac{\partial F}{\partial y} \mid (x, y) \in S_{Dom}\right\} &\simeq E\{S_{Dom}\} - E\{S\} \gg 0, \end{aligned} \quad (3.11)$$

while for the $\overline{S_{Dom}^n}$ set we get

$$\begin{aligned} E\left\{\frac{\partial F}{\partial x} \mid (x, y) \in \overline{S_{Dom}^n}\right\} &\simeq E\{\overline{S_{Dom}^n}\} - E\{S\} \approx 0 \\ E\left\{\frac{\partial F}{\partial y} \mid (x, y) \in \overline{S_{Dom}^n}\right\} &\simeq E\{\overline{S_{Dom}^n}\} - E\{S\} \approx 0 \end{aligned} \quad (3.12)$$

Hence,

$$E_{S_{Dom}^n}\{\nabla F_n\} \gg E_{\overline{S_{Dom}^n}}\{\nabla F_n\} \quad (3.13)$$

3.4 Convergence condition

By decomposing $\underline{\nabla} F_n$ according to the i th pixel's relation to either S_{Dom}^n or $\overline{S_{Dom}^n}$ we get

$$\begin{aligned}
\nabla_{\underline{P}} F &= \sum_{(x_i, y_i) \in S(\underline{P})} X_i \nabla F_n(x_i, y_i) \\
&= \sum_{(x_i, y_i) \in S_{Dom}^n} X_i \nabla F_n(x_i, y_i) + \sum_{(x_i, y_i) \in \overline{S_{Dom}^n}} X_i \nabla F_n(x_i, y_i) \\
&= \nabla_{\underline{P}} F_n^{Dom} + \nabla_{\underline{P}} F_n^{\overline{Dom}}
\end{aligned} \tag{3.14}$$

where $\nabla_{\underline{P}} F_n^{Dom}$ and $\nabla_{\underline{P}} F_n^{\overline{Dom}}$ correspond to dominant and non-dominant pixel sets respectively.

Next we calculate $E\{\nabla_{\underline{P}} F_n\}$, the expectancy of $\nabla_{\underline{P}} F$:

$$\begin{aligned}
E\{\nabla_{\underline{P}} F_n\} &= \sum_{(x_i, y_i) \in S_{Dom}^n} E\{X_i \nabla F_n(x_i, y_i)\} + \sum_{(x_i, y_i) \in \overline{S_{Dom}^n}} E\{X_i \nabla F_n(x_i, y_i)\} \\
&= E\{X_i\} \left(\sum_{(x_i, y_i) \in S_{Dom}^n} E\{\nabla F_n(x_i, y_i)\} + \sum_{(x_i, y_i) \in \overline{S_{Dom}^n}} E\{\nabla F_n(x_i, y_i)\} \right) \\
&= E\{X_i\} \left(|S_{Dom}^n| E_{S_{Dom}^n} \{\nabla F_n\} + |\overline{S_{Dom}^n}| E_{\overline{S_{Dom}^n}} \{\nabla F_n\} \right)
\end{aligned} \tag{3.15}$$

and the spatial distributions of S_{Dom}^n and $\overline{S_{Dom}^n}$ are assumed to be similar and independent of the gradient values.

Therefore, the convergence condition is given by:

$$|S_{Dom}^n| E_{S_{Dom}^n} \{\nabla F_n\} \gg |\overline{S_{Dom}^n}| E_{\overline{S_{Dom}^n}} \{\nabla F_n\} \tag{3.16}$$

By substituting Eq. 3.13 into Eq. 3.16 we get that convergence is achieved for:

$$|S_{Dom}^n| \geq |\overline{S_{Dom}^n}| \tag{3.17}$$

We conclude that the iterative optimization scheme converges when the initial estimate used, provides registration of a small part of the chosen pixels set S_2 to its true S_1 locations. The size of the initially aligned set, is given by:

$$|S_{Dom}^n| \gg (|S_1| - |S_{Dom}^n|) \frac{E_{\overline{S_{Dom}^n}} \{\nabla F_n\}}{E_{S_{Dom}^n} \{\nabla F_n\}} \tag{3.18}$$

Hence,

$$|S_{Dom}^n| \gg |S_1| \frac{E_{\overline{S_{Dom}^n}} \{\nabla F_n\}}{E_{\overline{S_{Dom}^n}} \{\nabla F_n\} + E_{S_{Dom}^n} \{\nabla F_n\}} \approx |S_1| \frac{E_{\overline{S_{Dom}^n}} \{\nabla F_n\}}{E_{S_{Dom}^n} \{\nabla F_n\}} \tag{3.19}$$

The smaller the ratio in intensity expectancies $\frac{E_{S_{Dom}^n}\{\nabla F_n\}}{E_{S_{Dom}^n}\{\nabla F_n\}}$, the smaller the set $|S_{Dom}^n|$ to be used. Thus, the sharper the image used for the iterative optimization, the larger the convergence range.

4 Experimental results

Several image pairs acquired by medical and remote sensing applications were registered using an affine and projective parametric motion models. In order to demonstrate the alignment, the high-gradient magnitude pixel set was overlaid on both images, where the initial estimate of the motion is given by its pixel overlay. A linear multi-resolution pyramid (Section 2.4) with 3 scales was used. Figure 2 shows the registration of medical multi-modality images using an affine motion model. These images are characterized by low noise and sharp contrast between the dominant and non-dominant sets. Thus, according to Eq. 3.19 these images can be registered using a small set of corresponding dominant pixels S_{Dom}^n and a less accurate initial estimate. Figure 3 shows the affine registration results of the severely dissimilar and noisy multi-sensor images, in this case, the ratio $\frac{E_{S_{Dom}^n}\{\nabla F_n\}}{E_{S_{Dom}^n}\{\nabla F_n\}}$ is not small due to the presence of non-mutual image features and thus, a relatively accurate initial estimate is needed. The registration results of these images, using the projective motion model are presented in Figure 4. The images in Figure 5 are taken from [3]. In this scenario there is a small number of non-mutual image feature, but the estimated motion is large.

5 Discussion

In this work a robust multi modality image registration algorithm was presented. The algorithm uses an implicit geometrical similarity measure which is invariant to intensity dissimilarities. The registration is achieved by tracking the migration of high-gradient pixels using robust global optimization. The convergence analysis leads to the derivation of an analytic convergence criterion. The experimental results demonstrate the effectiveness of the proposed algorithm by registering real multisensor and multi-modality images.

References

- [1] W. M. Wells III, P. Viola, H. Atsumi, S. Nakajima, and R. Kikinis, “Multi-modal volume registration by maximization of mutual information”, *Med. Image Anal.*, vol. 1, no. 1, pp. 35-51, 1996.

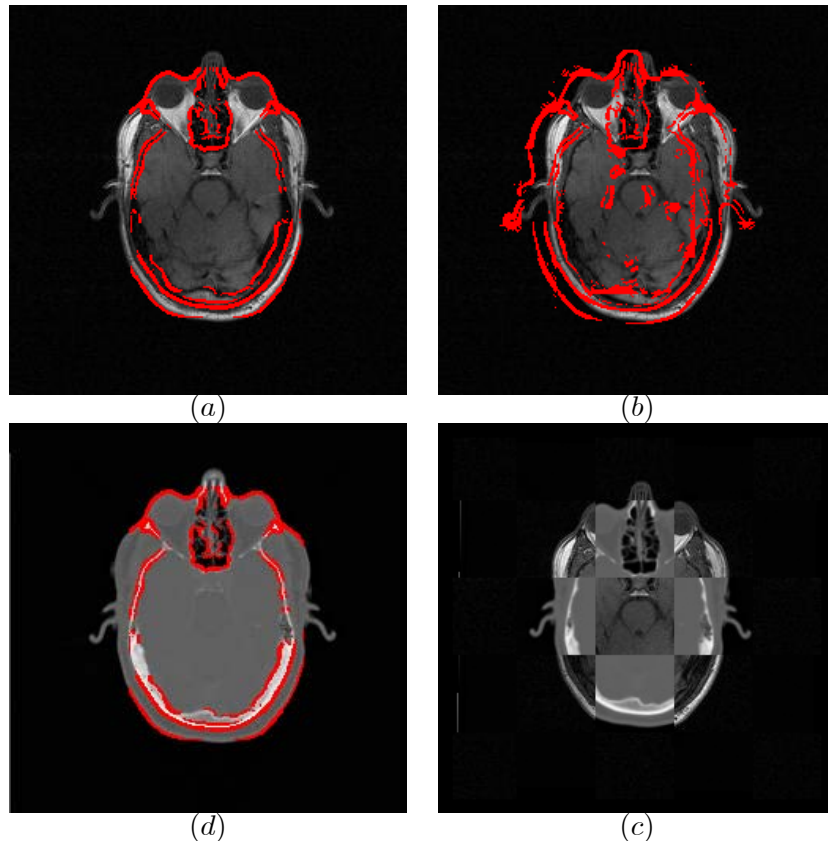


Figure 2: Registration results of CT and MRI multi-modality images using the affine motion model: (a) original MRI image overlaid with the set of high-gradient pixels . (b) Initial estimate of the overlaid set in the CT image. (c) Composite image. (d) Final alignment of the pixel set after migration.

- [2] Josien Pluim, J. B. Maintz and M.Viergever. “Image Registration by Maximization of Combined Mutual Information and Gradient Information”, IEEE Transactions on Medical Imaging, VOL. 19, NO. 8, August 2000.
- [3] M. Irani and P. Anandan, “Robust Multi-Sensor Image Alignment”. IEEE International Conference on Computer Vision (ICCV), India, January 1998.
- [4] H. Li, B.S. Manjunath, and S.K. Mitra, “A Contour Based Approach to Multisensor Image Registration”, IEEE Trans. Image Processing, vol. 4, pp. 320-334, March 1995.
- [5] J. Maintz, M. Viergever, “An Overview of Medical Image Registration Methods”, ftp://cs.uu.nl/people/twan/brussel_bvz.pdf
- [6] M. Irani and P. Anandan. “All About Direct Methods”, <ftp://ftp.robots.ox.ac.uk/pub/outgoing/phst/summary.ps.gz> .

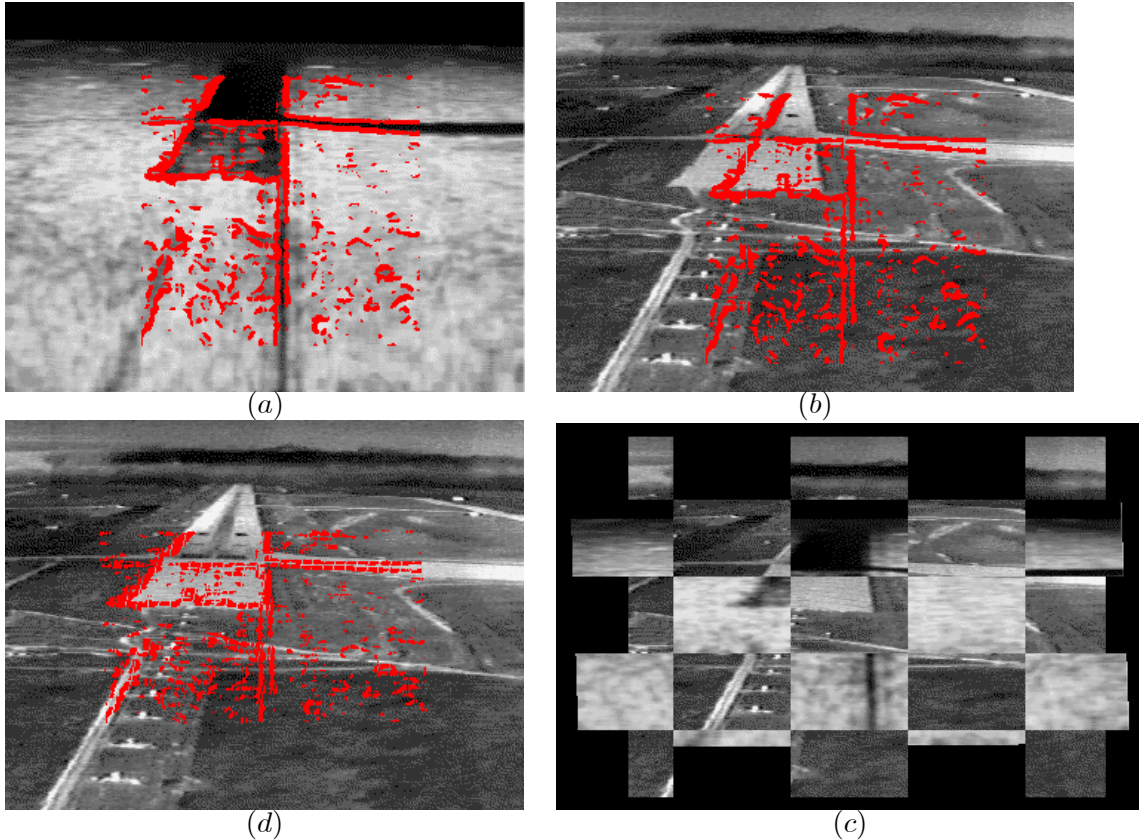


Figure 3: Registration results of SAR and FLIR multi-sensor images using the affine motion model: (a) original SAR image overlaid with the set of high-gradient pixels . (b) Initial estimate of the overlaid set in the FLIR image. (c) Composite image. (d) Final alignment of the pixel set after migration.

- [7] L. Brown, “A survey of image registration techniques”, ACM Computer Surveys, vol. 24(4), pp. 325-376, 1992.
- [8] R. Sharma and M. Pavel, “Registration of video sequences from multiple sensors” in Proceedings of Image Registration Workshop, Publication CP-1998-206853, NASA-GSFC, November 1997.
- [9] A. Guziec, X. Pennec, N. Ayache “Medical Image Registration Using Geometric Hashing”, IEEE Computational Science and Engineering, October-December 1997 (Vol. 4, No. 4), pp. 29-41.
- [10] P. Gill , “Practical Optimization”, Academic Press, 1982.
- [11] A. Averbuch, Y. Keller, “Fast motion estimation using bidirectional gradient methods”.

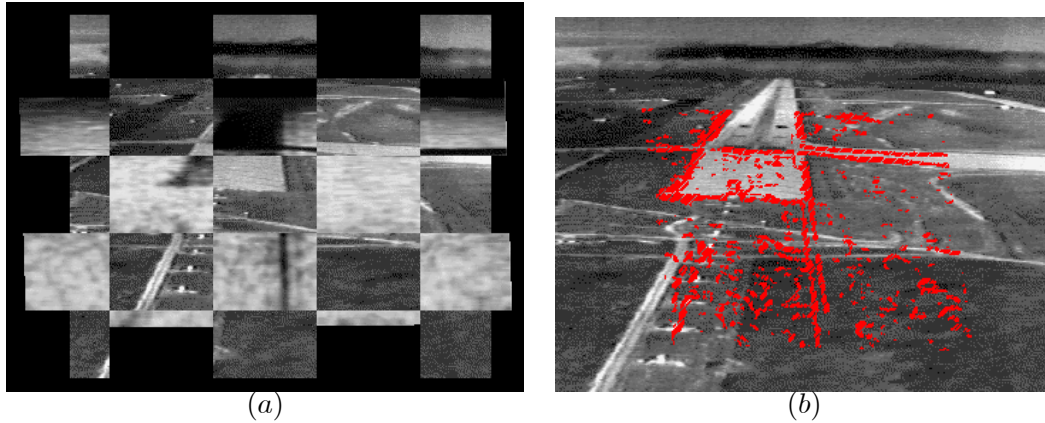


Figure 4: Registration results of SAR and FLIR multi-sensor images using the projective motion model: (a) Composite image. (b) Final alignment of the pixel set after migration. The initial pixel set and its initial projection are the same as in Figure 4.

- [12] E. Simoncelli and E. Adelson, "Noise removal via Bayesian wavelet coring", 3rd IEEE Int'l Conf on Image Processing. Lausanne Switzerland, September 1996.

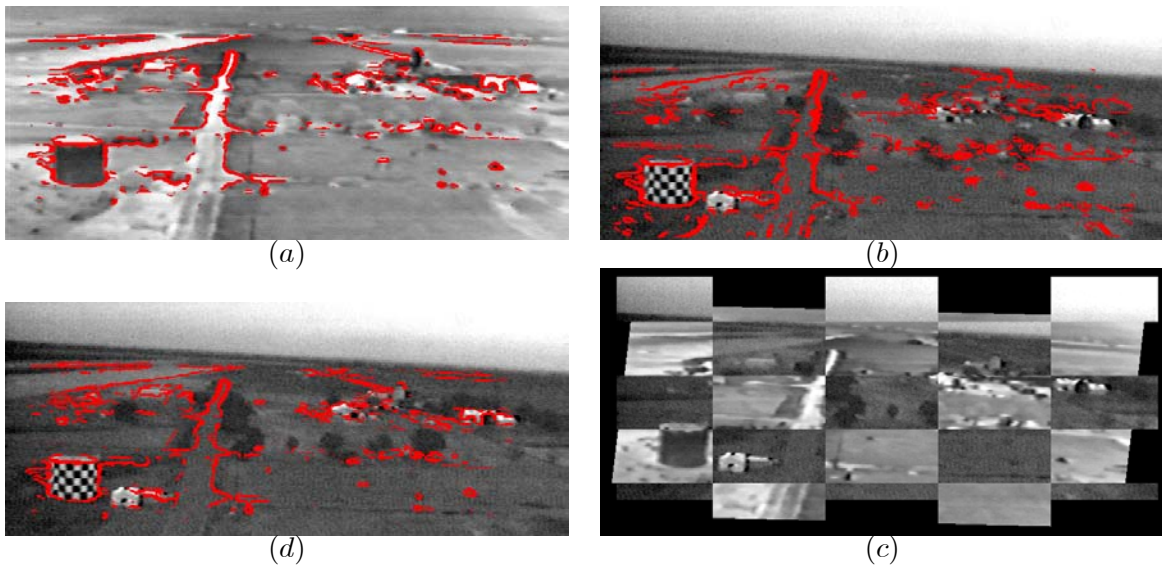


Figure 5: Registration results of EO and IR multi-modality images presented in [3] using the affine motion model: (a) original IR image overlaid with the set of high-gradient pixels . (b) Initial estimate of the overlaid set in the EO image. (c) Composite image. (d) Final alignment of the pixel set after migration.